Interlayer Arrangement of Hydrated MgAl Layered Double Hydroxides Containing Guest Terephthalate Anions: Comparison of Simulation and Measurement

Steven P. Newman,[‡] Samuel J. Williams,[†] Peter V. Coveney,*[,†] and William Jones[‡]

Schlumberger Cambridge Research, High Cross, Madingley Road, Cambridge, U.K. CB3 0EL, and Department of Chemistry, University of Cambridge, Lensfield Road, Cambridge, U.K. CB2 1EW

Received: March 10, 1998; In Final Form: May 27, 1998

The hydration of MgAl layered double hydroxides (LDHs) with interlayer terephthalate anions and controlled layer charge is studied. A combination of powder X-ray diffraction (PXRD), thermal gravimmetry (TG), and computer simulation is used to study in detail the effect of layer charge density and interlayer water content on the interlayer arrangement of the organo-LDH. For high water content and layer charge, an interlayer separation of approximately 14.0 Å is favored, which corresponds to a vertical orientation of the terephthalate anion with respect to the hydroxide layers. For low water content and layer charge, an interlayer separation of approximately 8.4 Å is favored, which corresponds to a horizontal terephthalate orientation. During cycles of dehydration−rehydration, PXRD indicates that the 14.0 and 8.4 Å units coexist in varying proportions depending on the layer charge and water content; in certain cases, a 22.4 Å interstratified phase consisting of a regular alternation of the 14.0 and 8.4 Å component interlayers can be identified. Molecular dynamics simulations predict a gradual expansion of the interlayer accompanied by a change in the orientation of the terephthalate anion from almost horizontal to vertical as the number of interlayer water molecules included in the simulation is increased. As the layer charge is increased, fewer water molecules are required to ensure a vertical terephthalate orientation, presumably as a consequence of the increased layer−layer Coulombic repulsion and interlayer packing density. There is, therefore, general agreement between the computer simulations and experimental measurements. The results demonstrate how the disposition of organic anions within the interlayer of organo-LDHs may be controlled.

1. Introduction

Layered double hydroxides (LDHs), also known as anionic clays, are host−guest materials that have recently received much attention because of their relevance in areas such as catalysis, medicine and oil-field technology.[1−5] The most important group of LDHs may be represented by the formula $[M^{2+}_{1-x}M^{3+}_{x}(OH)_2][^{x}/_{n}A^{n-}\cdot mH_2O]$, where M^{2+} and M^{3+} are divalent and trivalent cations, respectively, x is equal to the ratio $M^{3+}/(M^{2+} + M^{3+})$, and A is an anion of charge n. Observed M^{2+} and M^{3+} species include Mg^{2+}, Fe^{2+}, Co^{2+}, Cu^{2+}, Ni^{2+}, or Zn^{2+} and Al^{3+}, Cr^{3+}, Ga^{3+}, or Fe^{3+}, respectively. The structure of LDHs is most clearly described by considering the brucite-like structure, $M(OH)_2$, which consists of M^{2+} ions coordinated octahedrally by hydroxyl groups, with the octahedral units sharing edges to form infinite, charge neutral layers. In a LDH, isomorphous replacement of a fraction of the divalent cations with a trivalent cation occurs and generates a positive charge on the layers that necessitates the presence of interlayer, charge-balancing, anions. The remaining free space of the interlayer may be occupied by varying numbers of water molecules.

Although there is no significant restriction to the nature of the charge-balancing anion that can occupy the interlayer region, one subset of LDHs is that in which the charge-balancing anion is organic.[6,7] The incorporation of organic molecules between the layers of a LDH creates supramolecular structures[8] and is relevant in applications such as catalysis,[9−11] selective adsorption,[12,13] photochemistry,[14−16] and electrochemistry.[17−20] A particularly interesting aspect of organo-LDH chemistry is the effect of the layer charge density and degree of hydration of the LDH on the disposition of the organic anion between the layers.[16,21−24] An understanding of the factors controlling the interlayer arrangement is important if tailored applications in areas such as those mentioned above are to be found for organo-LDHs.

The charge density on the hydroxide layers of a LDH is dependent upon the M^{2+}/M^{3+} ratio (R) of the matrix cations in the layers. The anion-exchange capacity, and hence number and arrangement of the charge-balancing anions in the LDH, may therefore be controlled by varying R. In the present report, the interlayer arrangement of a LDH containing Mg and Al matrix cations with $R = 2$ or 3 and terephthalate interlayer anions is studied (abbreviated as MgAl(terephthalate) LDH $R(2)$ or $R(3)$). In particular, the effect caused by changes in the degree of hydration of the LDH on the interlayer arrangement is studied in detail using a combination of computer simulation, powder X-ray diffraction (PXRD), and thermal gravimmetry (TG). In addition, the occurrence of a MgAl(terephthalate) LDH phase, which is thought to be an interstratification of 14.0 and 8.4 Å component (22.4 Å regular interstratified phase) interlayers, is investigated.[22,25]

The phenomenon of interstratification is well-documented for cationic clays. The dehydration−rehydration of Na-smectite[26] or Mg-vermiculite,[27] for example, occur through the formation of interstratified phases. The phenomenon of interstratification in anionic clays was first reported by Bookin and Drits who

[†] Schlumberger Cambridge Research.
[‡] University of Cambridge.

S1089-5647(98)01426-6 CCC: $15.00
Published on Web 08/11/1998

described the structure of a mixed carbonate/sulfate LDH as consisting of alternating carbonate and sulfate interlayers.[28] The first observation of interstratification in a LDH where a single species of anion is present was made by Vucelic et al. for a MgAl(terephthalate) LDH at 75 °C.[25] The interstratified phase was interpreted as an alternation of expanded and collapsed interlayers. Kukkapdapu et al.[29] have recently prepared a series of MgAl(terephthalate) LDHs and suggested the existence of an interstratified phase consisting of alternating terephthalate and impurity carbonate interlayers. Interstratification of expanded and collapsed interlayers in a MgAl(benzoate) LDH has also recently been reported.[22]

The purpose of the present paper is to bring together detailed experimental observations and computer simulations of the effect of degree of hydration and R on the disposition of the terephthalate anion within the LDH interlayer. First (section 4.1), the effect of water content and R on the interlayer arrangement as observed experimentally (PXRD and TG) is discussed. Second (section 4.2), computer-simulated swelling curves for the $R(2)$ and $R(3)$ LDHs, obtained by increasing the water content of the computer model in small steps, are presented. By comparing the computer simulation and experimental observations, we are able to obtain detailed insight into the variation of the interlayer spacing and molecular structure with R and water content.

2. Experimental Section

A MgAl(terephthalate) LDH with Mg/Al = 2 or 3 ($R(2)$ or $R(3)$) was prepared using the well-established constant pH coprecipitation method.[22] An aqueous solution containing 0.028 mol of $Al(NO_3)_3$ and a stoichiometric amount of $Mg(NO_3)_2$ was added dropwise to 0.140 mol of terephthalic acid dissolved in $NaOH_{(aq)}$ at pH 10. The pH was maintained at 10 by the simultaneous addition of 2M $NaOH_{(aq)}$. A 10-fold excess of terephthalate above the necessary stoichiometric amount required for charge neutrality was used in the reaction mixture to reduce the probability of incorporating competing nitrate anions into the product LDH. The reaction mixture was crystallized at 65 °C for 18 h, filtered, and washed with hot water.

To investigate the effect of water content on the interlayer spacing of the product LDH, PXRD and TG data of sample fractions taken from the product were recorded as the LDH was dried and subsequently rehydrated (Figure 1). PXRD patterns were collected in air at room temperature using a Phillips PW1710 diffractometer with Cu Kα radiation and Ni filter. A step scan of 0.05 deg from 2.5 to 30° 2θ at a rate of 0.05 deg s^{-1} was used. TG profiles were collected on a Polymer Laboratories TGA 1500 apparatus from room temperature to 1000 °C, with a heating rate of 10 °C min^{-1} in air.

After filtering, the $R(3)$ and $R(2)$ LDHs were left in air at room temperature and sample fractions were taken for PXRD and TG analysis after 1 and 36 h. The partially dried LDHs were then further dried in air at 65 °C for 24 h. The LDHs were removed from the drying oven and then allowed to rehydrate in air at room temperature. Sample fractions were analyzed after rehydrating the oven-dried LDHs for approximately 15 min, 24 h, and 1 week in air at room temperature. Finally, one further sample fraction was analyzed after leaving the oven dried and partially rehydrated $R(3)$ LDH in an atmosphere of 75% relative humidity (75% RH) for 1 week. The above measurements therefore provide a series of "snapshots" of the LDHs at various stages of hydration.

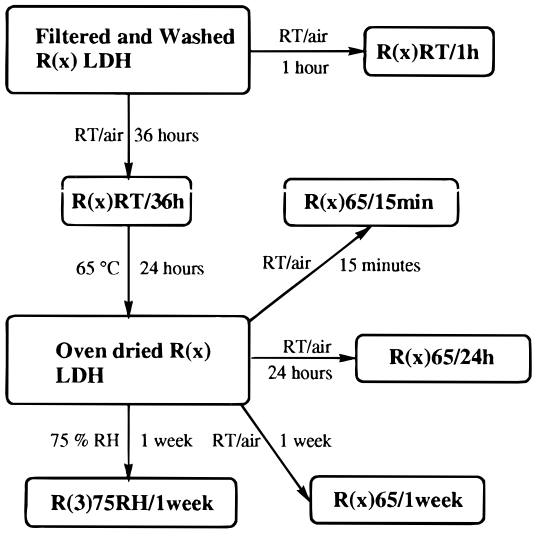

Figure 1. Scheme of the experimental routes followed to obtain different levels of hydration of MgAl(terephthalate) LDH $R(x)$, where $x = 2$ or 3. RT = room temperature, RH = relative humidity.

3. Simulation Methods

The model and interaction parameters are generally as described in previous simulations of LDHs, where full details of the simulation procedures and underlying theory are also presented.[30−33] The hydroxide layers of the simulation cell were constructed using the atomic positions from the crystal structure of naturally occurring hydrotalcite (a $MgAl(CO_3)$ LDH).[34] Hydroxide layers of size 18.30 × 9.15 Å^2 (equivalent to 18 unit cells in the *ab* plane) and 18.30 × 12.20 Å^2 (equivalent to 24 unit cells in the *ab* plane) were used for the $R(2)$ and $R(3)$ LDHs, respectively. The proportions of Mg and Al in the hydroxide layers were adjusted to give the correct Mg/Al ratio in each case. Simulation cells of different size were used so that an integer number of terephthalate anions per interlayer of each model were required for charge neutrality.[35] In both cases, two interlayers per periodic simulation cell with an initial interlayer separation of 14.4 Å were used. A stoichiometric number of terephthalate anions were positioned in an orientation approximately 45° to the normal direction from the layers. The appropriate number of water molecules were randomly positioned around the anions, with an equal number per interlayer of the simulation cell.

A modified version of the Dreiding force field[36] was used for the molecular simulations. The modification, originally introduced by Aicken et al.,[31] includes the addition of parameters not present in the original Dreiding force field for Mg and new parameters for water. The geometry and charges of the terephthalate anion were calculated using the MOPAC semiempirical method, employing the PM3 Hamiltonian.[37] The water geometry and charges were derived from the dedicated TIP3P water force field.[38] Charges on the atoms in the hydroxide layers were calculated using the charge equilibration (QEq) method.[39] The long range Coulombic interactions and the attractive van der Waals interactions were computed using the Ewald summation technique. Repulsive van der Waals interactions were treated with a direct cutoff radius of approximately 7 Å. Energy minimization was performed on all the models to remove close contacts prior to the molecular dynamics simulations.

Molecular dynamics (MD) simulations, with a time step of 0.001 ps, were performed in the constant composition, isothermal−isobaric (NPT) ensemble at 300 K. The temperature was

TABLE 1: Estimated Total Water Content of MgAl(terephthalate) *R*(3) LDH from TG Weight Loss up to 250 °C

sample	estimated % total water content	approx. equiv. no. of water molecules per simulation cell
R(3)RT/1h	83.9	≫80
R(3)RT/36h	14.9	36−40
R(3)65/15min	5.5	12−16
R(3)65/24h	12.8	28−32
R(3)65/1week	13.8	32−36
R(3)75RH	17.3	44−48

TABLE 2: Estimated Total Water Content of MgAl(terephthalate) *R*(2) LDH from TG Weight Loss up to 250 °C

sample	estimated % total water content	approx. equiv. no. of water molecules per simulation cell
R(2)RT/1h	81.6	≫64
R(2)RT/36h	21.3	44−48
R(2)65/15min	9.1	16−20
R(2)65/24h	17.7	36−40
R(2)65/1week	20.0	44−48

maintained using the Hoover thermostat[40] and the equivalent hydrostatic pressure was set to 10^5 Pa (1 atm). Periodic boundary conditions were applied in three dimensions. The effect of water content on the interlayer spacing of the LDH is simulated by increasing, in intervals of 4, the number of water molecules included in the simulation cell from 0 up to a maximum of 80. In the NPT ensemble, the volume of the system is allowed to vary, which enables the simulation to predict the interlayer spacing for a particular water content.

The total simulation time was generally 20 or 40 ps for the *R*(2) or *R*(3) LDHs, respectively (see results). Trajectory files with an update frequency of 0.1 ps were collected and the interlayer spacing for a particular water content was averaged over the last 10 ps of the MD simulation, after a thermal equilibration was adjudged to have been reached.

All of the above calculations were performed on a single node of a Silicon Graphics Origin 2000 machine comprising 20 R10000, 195 MHz processors, typically with a CPU time of no longer than 8 h for 20 ps of MD simulation.

The properties of the interlayer water in the *R*(3) and *R*(2) LDHs containing 64 and 44 water molecules (see results), respectively, were examined using data extracted from extended trajectory files of 0.5 ns MD simulations. The increased length of the simulation enables extraction of a reliable radial distribution function (RDF) and mean squared displacement (MSD) of the water molecules (O−O distances), owing to the improved statistics of longer MD runs. The water self-diffusion constant may also be determined from a linear fit of the MSD computed. Recent MD simulations of bulk water have found that a hybrid of the Dreiding and dedicated TIP3P water force fields, as used in the present work, yields structural parameters (such as RDF and the water self-diffusion constant) in good agreement with experimental values.[38] The extended LDH simulations were performed in parallel, across two nodes of the Origin 2000 with a CPU time of approximately 3 days.

4. Results

4.1. Experimental Measurement. The thermal decomposition of MgAl(terephthalate) LDHs may be divided into three stages of weight loss.[6,22] The first stage, up to approximately 250 °C, may be attributed to the loss of interlayer and external (interparticle) water. The second stage, from approximately 250 to 500 °C, is due to dehydroxylation of the layers, and the final stage, from approximately 480 to 600 °C, corresponds to decomposition of the interlayer terephthalate anions. The total water content (interlayer + external water) of the *R*(3) and *R*(2) LDHs may be estimated, therefore, from the measured weight loss up to 250 °C. The estimated total water contents from the TG profiles (Figure 1S) of the various LDH samples are recorded in Tables 1 and 2.

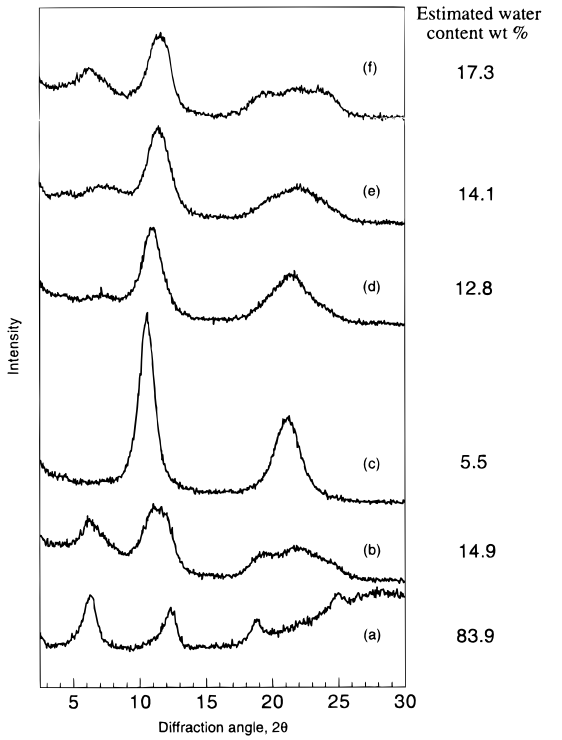

Figure 2. PXRD data showing the effect of water content on the interlayer spacing of MgAl(terephthalate) LDH *R*(3) (see Table 3): (a) RT/1h, (b) RT/36h, (c) 65/15 min, (d) 65/24h, (e) 65/1week, (f) 75RH/1week.

The theoretical formula of the LDH is $[Mg_{1-x}Al_x(OH)_2](TA^{2-})_{x/2}\cdot nH_2O$, where n depends on the degree of hydration of the LDH and $x = 0.25$ or 0.33 for *R*(3) or *R*(2), respectively. For *R*(3)65/1week (see Figure 1 for clarification of the nomenclature used), the measured weight loss up to 250 °C is 14.1%, which corresponds to $n = 2.90$ on the basis of the above theoretical formula. Elemental analysis of *R*(3)65/1week gives: **measured** 11.8% C, 0.0% N, 3.53% H; **calculated** 13.0% C, 0.0% N, 4.8% H. For *R*(2)65/1week, the measured weight loss up to 250 °C is 20.0%, which corresponds to $n = 3.60$ on the basis of the above theoretical formula. Elemental analysis of *R*(2)65/1week gives: **measured** 13.4% C, 0.0% N, 4.6% H; **calculated** 14.8% C, 0.0% N, 5.3% H. The slightly lower than expected observed carbon contents may indicate the presence of a small number of impurity CO_3^{2-} anions in the LDHs. The high affinity of LDHs for CO_3^{2-} is well-known.[3]

Figures 2 and 3 compare the PXRD patterns of the *R*(3) and *R*(2) LDHs, respectively, at various levels of hydration. Only the basal reflections are displayed, from which the interlayer spacing of the LDH may be deduced. The assignment of the basal reflections is given in Tables 3 and 4.

Three different LDH phases are identifiable across the series of PXRD patterns that correspond to either an expanded or collapsed interlayer structure, or what is generally thought to be an interstratification of expanded and collapsed interlayers. The "expanded phase" is identified by an interlayer spacing of

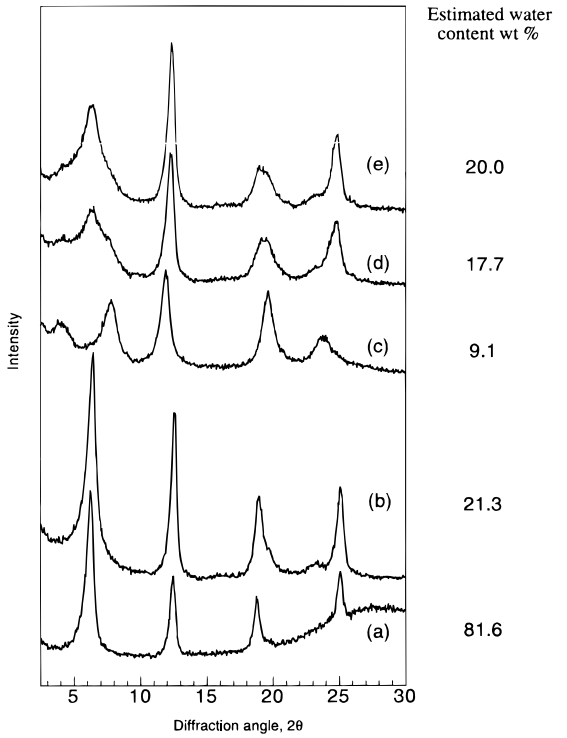

Figure 3. PXRD data showing the effect of water content on the interlayer spacing of MgAl(terephthalate) LDH *R*(2) (see Table 4): (a) RT/1h, (b) RT/36h, (c) 65/15 min, (d) 65/24h, (e) 65/1week.

TABLE 3: PXRD Data for MgAl(terephthalate) *R*(3) LDH (See Figure 3)[a]

sample	2θ obs	*d* obs/Å	assignment
R(3)RT/1h	6.27	14.10	001 E
	12.38	7.15	002 E
	18.76	4.73	003 E
	24.87	3.58	004 E
R(3)RT/36h	6.18	14.3	001 E
	11.34	7.8	002 E, 001 C
	19.30	4.6 sh	003 E
	21.68	4.1	002 C
	24.73	3.6 sh	004 C
R(3)65/15min	10.53	8.4	001 C
	21.15	4.2	002 C
R(3)65/24h	4.02	~22 vw	001 I
	7.37	12.3 vw	002 I, 001 E
	10.92	8.1	001 C
	21.15	4.2	002 C
R(3)65/1week	4.02	~22 vw	001 I
	7.19	~12 w	002 I
	11.34	7.8	002 E, 001 C, 003 I
	20.66	4.3 sh	003 E
	21.68	4.1	002 C
R(3)75RH	6.22	14.2	001 E
	11.49	7.7	002 E, 001 C
	19.73	4.5 sh	003 E
	21.68	4.1	002 C
	23.41	3.8	004 E

[a] E, C, and I indicate basal reflections from the expanded, collapsed, and interstratified phases, respectively. The presence of two or more assignments indicates complex reflections. sh = shoulder, w = weak reflection, vw = very weak reflection.

approximately 14 Å (6.31° 2θ), which corresponds to a gallery height of 9.2 Å following subtraction of the hydroxide layer thickness of 4.8 Å. Comparison of the length of the terephthalate anion with a gallery height of 9.2 Å indicates that the expanded phase corresponds to an approximately vertical orientation of the terephthalate anion with respect to the hydroxide layers. The "collapsed phase" is identified by an

TABLE 4: PXRD Data for MgAl(terephthalate) *R*(2) LDH (See Figure 4)[a]

sample	2θ obs	d obs/Å	assignment
R(2)RT/1h	6.41	13.80	001 E
	12.54	7.06	002 E
	18.92	4.69	003 E
	25.08	3.55	004 E
R(2)RT/36h	6.41	13.80	001 E
	12.54	7.06	002 E
	18.92	4.69	003 E
	25.08	3.55	004 E
R(2)65/15min	3.91	22.6	001 I
	7.78	11.36	002 I
	11.85	7.47	003 I
	19.60	4.53	005 I
	23.73	3.75	006 I
R(2)65/24h	3.91	22.6 w	001 I
	6.31	14.0	001 E
	7.76	11.4 sh	002 I
	12.27	7.21	002 E, 003 I
	19.34	4.59	003 E, 005 I
	24.73	3.60	004 E, 006 I
R(2)65/1week	6.31	14.0	001 E
	12.38	7.15	002 E
	19.30	4.60	003 E, 005 I
	24.73	3.60	004 E, 006 I

[a] E and I indicate basal reflections from the expanded and interstratified phases, respectively. The presence of two or more assignments indictates complex reflections. sh = shoulder, w = weak.

interlayer spacing of approximately 8.4 Å (10.53° 2θ), which corresponds to a gallery height of 3.6 Å and an approximately horizontal orientation of the terephthalate anion. The "interstratified phase" is identified by successive orders of basal reflections corresponding to a repeat distance of approximately 22.4 Å (3.94° 2θ)—the sum of the interlayer *d*-spacings of the expanded and collapsed phases.

4.1.a. MgAl(terephthalate) LDH R(3). The PXRD pattern of *R*(3)RT/1h (the freshly prepared *R*(3) LDH dried at room temperature for 1 h and with the highest total water content) exhibits a single LDH phase for which four orders of basal reflection can be resolved (Figure 2a). The reflections may be indexed on the basis of the expanded phase with an interlayer spacing of 14.1 Å (6.27° 2θ), thus suggesting that a vertical orientation of the terephthalate anions with respect to the hydroxide layers is preferred at high levels of hydration.

For *R*(3)RT/36h, obtained after drying the freshly prepared LDH at room temperature for 36 h (Figure 2b), the expanded LDH phase can still be identified by a 001 reflection at 14.3 Å (6.18° 2θ), although the reflection is broader and of lower intensity compared with the 001 reflection of *R*(3)RT/1h. The higher order basal reflections of *R*(3)RT/36h are also significantly broader compared with the basal reflections of *R*(3)RT/1h. In addition, the 002 reflection of *R*(3)RT/36h is more intense compared with *R*(3)RT/1h and is "shifted" to lower 2θ and toward the position of the 001 of the collapsed LDH phase. Furthermore, the 003 and 004 reflections are not completely resolvable and are also "shifted", in this case toward the position of the 002 reflection of the collapsed phase. These results suggest the existence of segregated domains of both the expanded and collapsed phases in *R*(3)RT/36h. Mild drying (room temperature) thus facilitates collapse of a small proportion of the interlayers, which then gives rise to the complex basal reflections observed. There is, however, no clear evidence for ordered interstratification, which would result in a reflection at approximately 22.4 Å (3.94° 2θ) and corresponding higher order reflections.

The PXRD pattern of the *R*(3) LDH with the lowest water content, *R*(3)65/15 min (Figure 2c), exhibits two relatively sharp and symmetric basal reflections, which may be indexed on the basis of the collapsed phase, with an interlayer spacing of 8.4 Å (10.53° 2θ). At low water content, therefore, a horizontal orientation of the terephthalate anions with respect to the hydroxide layers is preferred. After rehydration in air at room temperature for 24 h (*R*(3)65/24h), the collapsed phase can still be identified (Figure 2d), although the basal reflections are broader compared with *R*(3)65/15min. The broadening, along with very weak reflections at approximately 22 and 12 Å, indicates that a small proportion of the interlayers have expanded upon rehydration, with some degree of interstratification.

It should be noticed that despite the similar total water contents of *R*(3)RT/36h and *R*(3)65/24h (Table 3), the observed PXRD patterns are significantly different (i.e., contain different proportions of expanded and collapsed interlayers), indicating that a hysteresis loop exists during the dehydration−rehydration cycle.[41]

For *R*(3)65/1week, obtained by further rehydrating the oven-dried LDH in air at room temperature for 1 week, broad and weak reflections at approximately 22 (4.02° 2θ) and 12 Å (7.37° 2θ) indicate interstratification of expanded and collapsed interlayers, although the poor quality of the reflections shows that the interstratification is not well-ordered (Figure 2e). For *R*(3)75RH/1week, obtained by further rehydrating the LDH in an atmosphere of 75% relative humidity for 1 week (Figure 2f), a broad reflection at 14.0 Å (6.31° 2θ) indicates that although the water total water content is only slightly increased, a significantly higher proportion of the interlayers are expanded in this sample compared with *R*(3)65/1week.

The series of PXRD patterns indicate that a vertical (expanded interlayer) or horizontal (collapsed interlayer) arrangement of the terephthalate anion with respect to the hydroxide layers is preferred in the *R*(3) LDH at high or low interlayer water content, respectively. As the LDH is dried or rehydrated, a reversible reorientational phase change between a vertical and horizontal orientation of the terephthalate anion occurs. For intermediate water content, the complex basal reflections observed suggest that domains of the expanded and collapsed interlayers coexist, presumably corresponding to the coexistence of relatively hydrated and dehydrated interlayers in the LDH, respectively. The dehydration−rehydration of the LDH thus appears to occur in a nonuniform manner throughout the sample. In addition, there is some evidence for possible interstratification (i.e., weak, broad basal reflections corresponding to a repeat distance of approximately 22 Å in the *c*-direction) of the expanded and collapsed layers for intermediate water contents, indicating the alternation of hydrated and dehydrated layers within individual crystallites. It will be seen in the next section, however, that interstratification can be more clearly observed in the *R*(2) LDH, indicating higher ordering of the alternating layers compared with the *R*(3) LDH.

4.1.b. MgAl(terephthalate) LDH R(2). The PXRD pattern of *R*(2)RT/1h (the *R*(2) LDH with the highest total water content) exhibits a single LDH phase for which four orders of basal reflection are easily resolved (Figure 3a). The interlayer spacing of this phase is approximately 14 Å (6.31° 2θ), which corresponds to the expanded phase. The basal reflections are sharper and more intense compared with *R*(3)RT/1h (Figure 2a), indicating increased interlayer ordering of the expanded phase in *R*(2)RT/1h.

The water content of the *R*(2) LDH is much reduced following drying for 36 h in air (*R*(2)RT/36h), although the PXRD pattern is substantially unchanged (Figure 3b) compared with *R*(2)RT/1h. Following drying at 65 °C (*R*(2)65/15 min), however, which further reduces the water content of the LDH, all the reflections may be indexed on the basis of ordered interstratification of expanded and collapsed interlayers (Figure 3c). The sharpness of the reflections suggests that interstratification is more significant for the *R*(2) LDH compared with the *R*(3) LDH. Unlike the *R*(3) LDH, a phase with approximately all the interlayers collapsed is not observed for the *R*(2) LDH following drying at 65 °C.

After the oven-dried LDH was left in air at room temperature for 24 h (*R*(2)65/24h), the proportion of the expanded interlayers in the LDH has increased significantly, although some evidence of interstratification is still present (Figure 3d). By comparing the PXRD patterns for *R*(3)65/24h and *R*(2)65/24h (Figures 2d and 3d), it is clear that the collapsed interlayers in the *R*(2) LDH rehydrate and expand more readily than in the *R*(3) LDH.

Further rehydration of the oven-dried *R*(2) LDH further increases the number of expanded interlayers present; however, the interstratified phase may still be detected even after leaving the oven-dried LDH in air for 1 week (*R*(2)65/1week) indicating that a small proportion of the interlayers remain collapsed (Figure 3e). Although the total water content of *R*(2)65/1week is almost the same as *R*(2)RT/36h, the crystallinity of the expanded phase observed upon rehydration is not as high as that observed before drying at 65 °C, thus indicating hysteresis during the cycle of dehydration−rehydration.

4.2. Computer Simulation. Thermal equilibration of the MD simulations was judged to have been reached when variations in the calculated interlayer spacing became insignificant. For the *R*(2) LDH this generally occurred after approximately 10 ps, whence a further 10 ps of simulation time was used to calculate an average interlayer spacing. For the *R*(3) LDH, however, a large variation of the interlayer spacing generally continued to be observed beyond 10 ps, thus indicating that an equilibrium had not been achieved on this time scale. In these cases a further 20 ps of simulation was performed (making a total simulation time of 40ps) and average interlayer spacings were obtained from the last 10 ps of the extended simulation. The longer relaxation time required for the *R*(3) LDH is due, at least in part, to the larger size of simulation cell used, compared with the *R*(2) LDH.

Before comparing the experimental observations described in the previous section with the results of the computer simulations, it is necessary to highlight the important practical differences between the two. The most significant difference is that the experimental measurements are performed on open systems (N is not fixed), whereas the simulations are of closed systems (N is fixed). In the NPT ensemble, the computer model contains, by construction, fixed and equal numbers of both water molecules and terephthalate anions in each interlayer of the simulation cell. In the real system, however, the composition of each interlayer is not fixed nor, in fact, precisely known. The water content measured experimentally, for example, is the total water content (interlayer + interparticle water), whereas the computer simulations consider only interlayer water. In the open system, water is free to diffuse between the interlayer, pore space, and surroundings, whereas in the closed system the interlayer water content is fixed. Furthermore, experimental evidence suggests that in certain cases hydrated and dehydrated interlayers coexist, whereas a symmetric distribution of water is imposed for the computational models (see section 4.3).

The presence of a small number of impurity carbonate anions in the real system as well as variations in *R* may also be

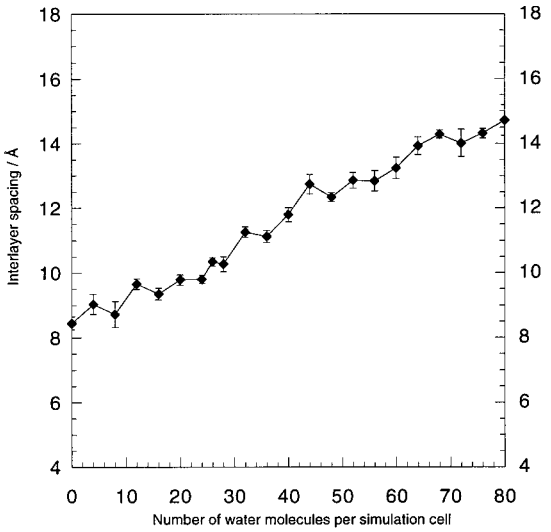

Figure 4. Simulated swelling curve for MgAl(terephthalate) LDH *R*(3).

important. Consideration of these factors when comparing the simulation and measurement is crucial to the understanding of the interlayer structure and behavior of LDHs.

4.2.a. MgAl(terephthalate) LDH R(3). Figure 4 is the simulated swelling curve obtained for the *R*(3) LDH, where the error bars represent the fluctuations about the average interlayer spacing (2 standard deviations in each direction) within the equilibrated region. The small size of the fluctuations about the average interlayer spacing suggests that the model structures have reached thermal equilibration. The interlayer spacing increases gradually from approximately 8.5 Å for 0 interlayer water content up to approximately 15 Å for 80 water molecules. The gradual expansion of the interlayer with increasing water content is accompanied by a gradual change in the orientation of the terephthalate anions from horizontal to vertical. All of the simulations up to and including 72 water molecules show the terephthalate anion to be bridging the interlayer region by hydrogen bonding to the hydroxyl groups on each surface.

Figure 5a shows the interlayer arrangement of the *R*(3) LDH after 40 ps of molecular dynamics with 16 water molecules (approximately 7 wt %) at 300 K (the model in closest agreement, in terms of water content and interlayer spacing, with *R*(3)65/15 min). The computer model confirms that for low interlayer water contents, the terephthalate anions adopt an approximately horizontal arrangement with respect to the hydroxide layers−corresponding to the collapsed phase observed experimentally.

Comparison of the measured interlayer spacing of *R*(3)RT/1h with the swelling curve suggests an interlayer water content of approximately 20−25 wt % for this sample (approximately 64−72 water molecules per supercell). Figure 5b shows the interlayer arrangement of the *R*(3) LDH after 40 ps of molecular dynamics with 64 water molecules at 300 K. The terephthalate anion adopts a vertical orientation with respect to the hydroxide layers, with the carboxylate groups hydrogen bonded to the hydroxide surfaces. The computational model indicates that the measured total water content for *R*(3)RT/1h of 80 wt % is largely due to external (i.e., interparticle) surface water. Above 72 water molecules per supercell, the simulation predicts that the additional water molecules insert between the carboxylate groups of the terephthalate anions and the hydroxide surface causing further expansion of the interlayer to 15 Å and beyond. No such interlayer separation above 14.3 Å is detected experimentally, under ambient conditions of pressure and temperature, thus indicating that the additional water is condensed in the interparticle pore space. It is possible, however, that under conditions of high water vapor pressure the expansion of the

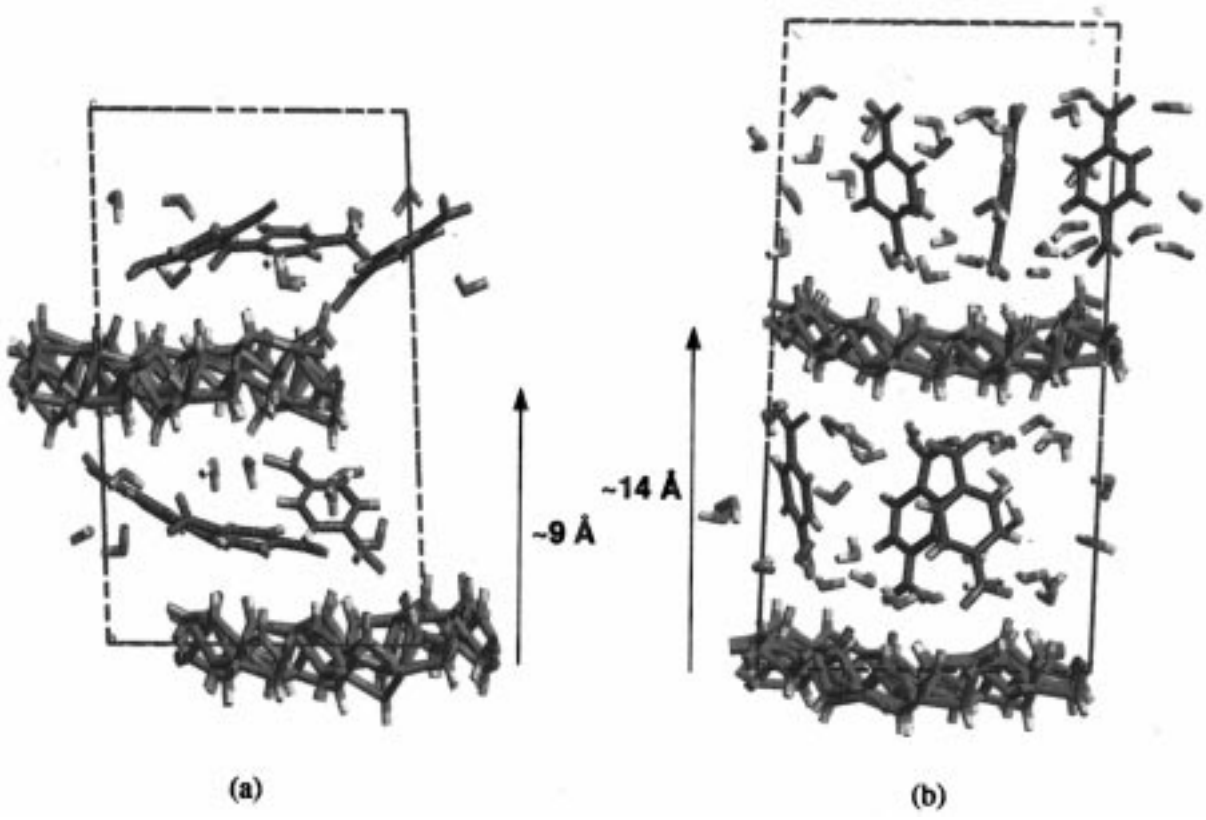

Figure 5. Snapshot of a simulation cell, following 40 ps of molecular dynamics at 300 K, containing MgAl(terephthalate) LDH *R*(3) with (a) 16 water molecules and (b) 64 water molecules.

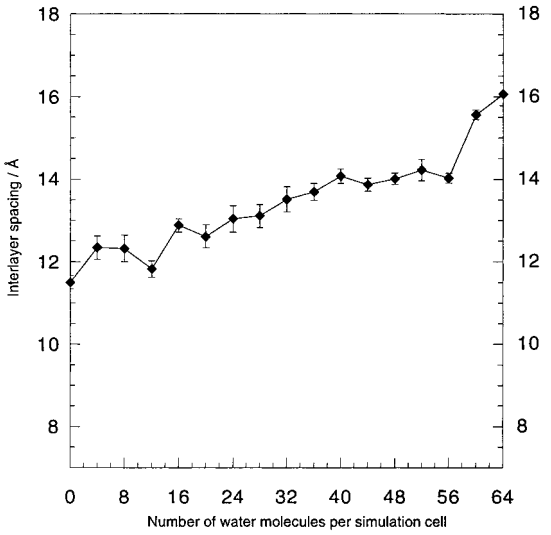

Figure 6. Simulated swelling curve for MgAl(terephthalate) LDH *R*(2).

interlayer to 15 Å and beyond, as predicted by the computer simulations, may occur.[33]

From the water contents measured for *R*(3)RT/36h and *R*(3)-75RH/1week, the simulations predict an interlayer spacing slightly lower (1−2 Å) than the measured interlayer of the expanded phase, which is the dominant phase in these samples. The predicted interlayer spacings of *R*(3)65/24h and *R*(3)65/1week are approximately halfway between the interlayer spacing measured for the expanded and collapsed phases, with the terephthalate anions inclined at an angle of approximately 40° to the normal direction from the layers. The PXRD patterns of these samples, however, suggests the coexistence of the expanded and collapsed phases.

4.2.b. MgAl(terephthalate) LDH R(2). Figure 6 is the simulated swelling curve obtained for the *R*(2) LDH. At first, the interlayer spacing increases gradually with increasing water content, before leveling off between 40 and 56 water molecules at a *d*-spacing of approximately 14.0 Å. All of the simulations up to and including 56 water molecules show the terephthalate anions to be bridging the interlayer region by hydrogen bonding to hydroxyl groups on each surface. At low water content the terephthalate anions are inclined at an angle of approximately 45° with respect to the normal of the layers, rather than an approximately horizontal orientation as simulated for *R*(3). Between 40 and 56 water molecules the terephthalate anions are in an approximately vertical orientation with respect to the hydroxide layers—corresponding to the expanded interlayer structure observed experimentally. Above 60 water molecules, however, each terephthalate anion is detached from one layer and water molecules insert themselves between the carboxylate groups and the hydroxide layer; there is a concomitant increase in interlayer spacing to about 15.5 Å.[33]

For *R*(2)RT/36h, *R*(2)65/24h, and *R*(2)65/1week, which predominantly consist of expanded interlayers, the measured water contents correspond to between approximately 36 and 46 water molecules per simulation cell. In the region of the swelling curve between contents of 36 and 56 water molecules, the predicted interlayer spacing is approximately 14.0 Å (with the terephthalate anions in an approximately vertical orientation), in good agreement with the experimentally observed interlayer spacing of the expanded phase.

4.3. Interlayer Structure and Interstratification. The interlayer arrangement of the terephthalate anion in a MgAl-(terephthalate) LDH is evidently dependent upon the Mg/Al ratio (i.e., the charge density on the layers) and the water content of the LDH. For both the *R*(3) and *R*(2) LDHs, simulation and experiment confirm that a vertical orientation of the terephthalate anion with respect to the hydroxide layers is preferred at high interlayer water content. After the *R*(3) LDH is dried at 65 °C, approximately all of the interlayers are collapsed. For the *R*(2) LDH, however, drying at 65 °C produces an ordered interstratification of expanded and collapsed interlayers. After the dried LDHs are left in air, comparison of the PXRD patterns of *R*(3)-65/24h (Figure 3d) and *R*(2)65/24h (Figure 4d) shows that the collapsed interlayers of the *R*(2) LDH rehydrate and expand more readily compared with the *R*(3) LDH.

The different behavior of the *R*(2) and *R*(3) LDHs upon drying and rehydration is certainly due to the different charge density on the layers of the LDHs. The charge density is highest for the *R*(2) LDH, owing to increased substitution of Al^{3+} for Mg^{2+} compared with the *R*(3) LDH. Increased charge density on the layers results in stronger Coulombic repulsion between the layers and increased packing of anions between the layers—factors that both enhance the propensity for the terephthalate anions to adopt a vertical orientation.

The closest agreement between the experimental measurements and the simulated swelling curves is obtained for samples that consist of approximately 100% expanded or collapsed interlayers, respectively. For the samples that consist of expanded and collapsed interlayers simultaneously, comparison with the simulated swelling curves is less straightforward. The canonical aspect (fixed N) of the simulations makes it impossible to predict situations where such changes can occur.

Ordered interstratification of the expanded and collapsed interlayers is most clearly observed for *R*(2)65/15min, for which the measured water content corresponds to approximately 20 water molecules per supercell. From the *R*(2) swelling curve (Figure 6), the predicted interlayer spacing for a model with 20 water molecules is approximately 12.5 Å, which is intermediate between the interlayer spacing of the expanded and collapsed layers. In the simulation, each of the two interlayers in the supercell has an approximately equal interlayer spacing, with the terephthalate anions inclined at an angle of approximately 45° to the normal of the hydroxide layers. Experimentally, however, the existence of the interstratified phase suggests an ordered alternating sequence of relatively hydrated and dehydrated interlayers, with the terephthalate anions in either a vertical or horizontal orientation, respectively. In the NPT ensemble, the simulation cannot predict a model with alternating layers of expanded (hydrated) and collapsed (dehydrated) interlayers owing to the imposed symmetric distribution of interlayer water.

To further investigate the occurrence of interstratification, two additional 20 ps MD simulations were performed on *R*(2) models with unequal distributions of water molecules between the two interlayers of the simulation cell. The distributions 20:0 and 15:5 were used so that in both cases the total water content of the simulation cell was 20 water molecules.

Figure 7 compares the experimental PXRD pattern of *R*(2)-65/15min with simulated PXRD patterns of the models with equal (denoted 10:10) and unequal (denoted 15:5 and 20:0) interlayer water distribution, following 20 ps of MD simulation. The simulated patterns are calculated, using Cu Kα radiation ($\lambda = 1.5418$ Å), from the atomic positions of the final models at the end of the MD simulations.[30] The simulated pattern of the symmetric 10:10 model (Figure 7b), with a 001 reflection at 12.8 Å (6.91° 2θ) indicates an equal layer separation of the two interlayers in the simulation cell. The simulated PXRD

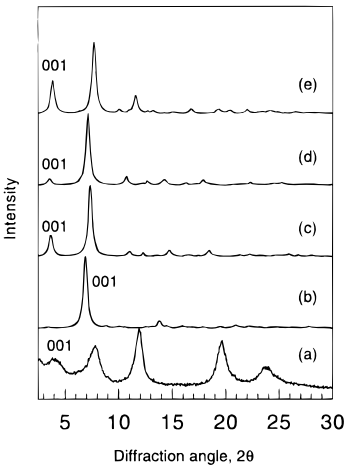

Figure 7. Comparison of experimental PXRD data for (a) *R*(2)65/15min and simulated PXRD data for the computer simulated models (b) 10:10, (c) 15:5, (d) 20:0, and (e) 20:0/CO_3 (see text). A crystallite size of $a = 500$, $b = 500$, and $c = 200$ Å was used in the PXRD simulations to obtain qualitative agreement with the experimentally observed peak widths.

TABLE 5: Effect of Water Distribution on the Calculated Enthalpy, *H*, and Coulombic Interaction Energy, *C*, of MgAl(terephthalate) *R*(2) LDH with 20 Water Molecules Per Simulation Cell

water distribution per interlayer	H/kcal mol^{-1}	C/kcal mol^{-1}
10:10	-8590 ± 20	$-17\,950 \pm 20$
15:5	-8540 ± 20	$-17\,900 \pm 20$
20:0	-8531 ± 20	$-17\,870 \pm 20$

patterns of the 15:5 and 20:0 models (parts c and b of Figure 7, respectively) with 001 reflections at approximately 24 Å (3.68° 2θ) indicate unequal separation of the two interlayers in the simulation cell and, consequently, an interstratified-like arrangement. For the 15:5 and 20:0 models, the smaller interlayer separation is observed for the interlayers with the lowest water content, as would be expected.

The enthalpy, $H = U + PV$, of the models may be determined by averaging the total internal energy of the system (U is the sum of the total kinetic and potential energies for the system) over the final 10 ps of the MD simulations. Comparing the enthalpies of the 10:10, 15:5, and 20:0 models (Table 5) suggests that the symmetric distribution of water is energetically more stable than either of the asymmetric distributions.[42] Assuming the interstratified phase consists of alternating hydrated and dehydrated interlayers, the implication of the energy difference is that the interstratified phase observed experimentally is enthalpically metastable. Once the interstratified phase has formed it is long-lived and presumably separated from the true equilibrium state by large (compared with the thermal energy available at room temperature (RT at 300 K = 0.6 Kcal mol^{-1})) energy barriers. The Coulombic contributions to the enthalpies are also presented in Table 5. The relative values indicate that Coulomb interactions (e.g., repulsion between the positively charged hydroxide layers) are the dominant contribution to the calculated enthalpy differences.

The *d*-spacing of the 001 reflection predicted by the MD simulation of the *R*(2) asymmetric models (approximately 24 Å (3.68° 2θ)) is higher than the experimentally observed *d*-spacing of the 001 reflection of the *R*(2) interstratified phase (approximately 22 Å (4.02° 2θ). It should also be noticed that the occurrence of ordered interstratification in the *R*(2) LDH requires that approximately 50% of the layers are collapsed, with an interlayer spacing of approximately 8.4 Å. The computer simulation predicts, however, an interlayer spacing of 11.5 Å for the *R*(2) model with no interlayer water molecules present (Figure 6). One possible explanation for the difference is that there is insufficient space to pack the required number of terephthalate anions in a horizontal orientation in the *R*(2) LDH. In the NPT ensemble, where the number of terephthalate anions per interlayer is fixed, a larger interlayer spacing is consequently predicted as steric interactions prevent the terephthalate anions from adopting a horizontal orientation. In the real system, it is possible that a small proportion of the terephthalate anions diffuse to the edges of crystallites as the layers collapse, thereby creating enough space for the remaining interlayer anions to adopt a horizontal orientation. Alternatively, the presence of a small number of impurity carbonate anions may reduce the steric interactions, thus facilitating layer collapse.

Figure 7e is the simulated PXRD pattern, following 20 ps of MD simulation, of the *R*(2) model with a 20:0 water molecule distribution, in which a single terephthalate anion in one interlayer has been replaced with a carbonate anion (denoted 20:0/CO_3). In this case, there is excellent agreement between the calculated and observed *d*-spacings. The agreement between the calculated and observed relative intensities is also significantly improved, compared with the pure terephthalate model. The improvement demonstrates the possible effect of steric interactions between the interlayer terephthalate anions upon the interlayer arrangement.

4.4. Properties of Interlayer Water. For the *R*(3) model with 64 water molecules, the majority of the water molecules form a monolayer on each of the hydroxide layer surfaces (Figure 5b). A small proportion of the water molecules also occupy the hydrophobic midplane of the interlayer. It is interesting to notice that relatively mild drying of the LDHs (65 °C) is sufficient to induce collapse of the interlayers. The interlayer water responsible for the expansion of the interlayers must, therefore, be weakly bound and easily removed from the interlayer. It is probable that this water occupies the hydrophobic midplane of the LDH interlayer.

The properties of the interlayer water in the expanded LDH phases were further examined using data extracted from trajectory files of 0.5 ns MD runs on the *R*(3) and *R*(2) models containing 64 and 44 water molecules, respectively. For both the *R*(3) and *R*(2) models, the calculated interlayer spacing and internal energy (U) are unchanged following the extended MD simulation compared with the initial 40 or 20 ps runs, respectively. The invariance of the interlayer spacing and U confirm that equilibration of the systems has been reached following the initial 40 or 20 ps MD simulations. The simulated water O−O RDF for the *R*(3) model with 64 water molecules (Figure 2Sa in the Supporting Information) is very similar to that obtained by Boek et al. from simulations of bulk water.[38] A large, sharp peak at 2.9 Å and a broad, weak peak at approximately 5.6 Å in the O−O RDF represent the first and second coordination shells of water, respectively, probably within a single surface water monolayer. The water self-diffusion constant, D, calculated for all the water molecules in the model ($D = 4.41 \times 10^{-7}$ cm^2 s^{-1} per atom) is the same order of magnitude as experimental data ($D = 2.47 \times 10^{-7}$ per atom at 50 °C) obtained using quasi elastic neutron scattering.[33,43] As would be expected for water constrained between the layers of a LDH, the calculated water self-diffusion constant is significantly lower than the value obtained from simulations of bulk water ($D = 1.88 \times 10^{-5}$ cm^2 s^{-1} per atom).[38]

The distribution of water in the *R*(2) model with 44 water molecules is very similar to the distribution of water in the expanded interlayer *R*(3) model (64 water molecules) described above. The peak at 5.6 Å in the water O−O RDF of the *R*(2) model (Figure 2Sb) is more defined than the peak observed for the second coordination shell of water in the expanded interlayer *R*(3) model. An additional broad, weak peak at approximately 7.5 Å, which corresponds to O−O distances between the water monolayers, is also observed in the water O−O RDF of the *R*(2) model, thus indicating increased structural ordering of the water molecules in the *R*(2) model compared with *R*(3). The higher degree of ordering of the water molecules in the *R*(2) model is most likely related to the increased charge density on the hydroxide layers of the *R*(2) LDH and consequent stronger attachment of the water molecules to the hydroxide layers. Furthermore, the water self-diffusion constant, calculated for all the water molecules in the model ($D = 1.14 \times 10^{-7}$ cm^2 s^{-1} per atom) is lower than the water-self-diffusion constant calculated for the *R*(3) model, indicating lower water mobility in the *R*(2) model compared with the expanded interlayer *R*(3) model—a feature that is also readily understood in terms of the relative charge densities of the layers (the higher the charge density, the more tightly bound the water molecules).

5. Conclusions

Experimental measurements and computer simulations have demonstrated that the orientation of the terephthalate anion within a MgAl(terephthalate) LDH is strongly dependent upon the hydroxide layer charge and the interlayer water content of the LDH.

For high water content and layer charge (i.e., *R*(2)) an interlayer separation of approximately 14.0 Å is favored, which corresponds to a vertical orientation of the terephthalate anion with respect to the hydroxide layers. For low water content and layer charge (i.e., *R*(3)), an interlayer separation of approximately 8.4 Å is favored, which corresponds to a horizontal terephthalate orientation. During cycles of dehydration−rehydration, PXRD indicates that the 14.0 and 8.4 Å interlayers coexist in varying proportions, depending on the layer charge and water content of the LDH. In certain cases, a 22.4 Å phase has been interpreted as consisting of an ordered interstratification of the 14.0 and 8.4 Å component interlayers. From a practical perspective, the results indicate that, in general, the interlayer water content of organo-LDHs should be carefully considered in the interpretation of PXRD data.

Computer simulation shows that for a *R*(2) LDH, a minimum of approximately 20 water molecules per interlayer of the simulation cell is required to ensure a vertical orientation of the terephthalate anion. A correspondingly larger number of water molecules are required for the *R*(3) LDH (approximately 32 water molecules per interlayer), owing to the lower layer charge and interlayer anion packing density, compared with the *R*(2) LDH. There is, therefore, general agreement between the computer simulations and the experimental measurements.

Computer simulations on models with unequal numbers of water molecules in adjacent interlayers support the experimental interpretation that the interstratified phase consists of alternating relatively dehydrated and hydrated interlayers. The interstratified phases are probably, therefore, formed during dehydration−rehydration by the removal or addition of water in a nonuniform manner throughout the LDH crystallites. Furthermore, energy calculations of models containing equal and unequal water distributions suggest that the observed interstratified phases are metastable.

The comparison between the experimental measurements and computer simulations has provided detailed insight into the interlayer properties of MgAl(terephthalate) LDHs. The simulations have helped to clarify various aspects of the experimental work and are a valuable adjunct for the interpretation of experimental data. It may be expected that the interlayer arrangement of LDHs containing guest species other than terephthalate are equally sensitive to variation in layer charge, degree of hydration, and the various other factors discussed in this paper.

Acknowledgment. The authors thank Molecular Simulations Inc. for facilitating access to some of the simulation software and Schlumberger Cambridge Research Ltd. and the EPSRC for financial support (CASE Award to S.P.N.).

Supporting Information Available: Representative TG profiles of the *R*(3) and *R*(2) MgAl(terephthalate) LDHs (Figure 1S), and the simulated water O−O RDF for the *R*(3) and *R*(2) models with 64 and 44 water molecules, respectively (Figure 2S). Ordering and accessing information is given on any current masthead page.

References and Notes

(1) Lavoix, F.; Lewis, M. *Oil Gas J.* **1992**, *92* (*Sept. 28*), 87.
(2) Fraser, L.; Enriquez, F. *Pet. Eng. Int.* **1992**, *June*, 43.
(3) Cavani, F.; Trifirò, F.; Vaccari, A. *Catal. Today* **1991**, *11*, 173−301.
(4) de Roy, A.; Forano, C.; El Malki, K.; Besse, J.-P. In *Anionic Clays: Trends in Pillaring Chemistry, Synthesis of Microporous Materials*; Occeli, M. L., Robson, E. R., Eds.; Van Nostrand Reinhold: New York, 1992; Vol. 2, pp 108−169.
(5) Vaccari, A. *Appl. Clay Sci.* **1995**, *10*, 1−3.
(6) Newman, S. P.; Jones, W. *New J. Chem.* **1998**, 22, 105−115.
(7) Carlino, S. *Solid State Ionics* **1997**, *98*, 73−84.
(8) Jones, W.; Kooli, F.; Bovey, J.; Newman, S. P. In *The Latest Frontiers of Clay Chemistry: Proceedings of the Sapporo Conference on the Chemistry of Clays and Clay Minerals (Sapporo, Japan, 1996)*; Yamagishi, A., Aramata, A., Taniguchi, M., Eds.; the Smectite Forum of Japan: Sendai, Japan, 1998; pp 70−87.
(9) Carrado, K. A.; Forman, J. E.; Botto, R. E.; Winans, R. E. *Chem. Mater.* **1993**, *5*, 472−478.
(10) Chibwe, M.; Pinnavaia, T. J. *J. Chem. Soc., Chem. Commun.* **1993**, 278−280.
(11) Ukrainczyk, L.; Chibwe, M.; Pinnavaia, T. J.; Boyd, S. A. *Environ. Sci. Technol.* **1995**, *29*, 439−445.
(12) Dekany, I.; Berger, F.; Imrik, K.; Lagaly, G. *Colloid Polym. Sci.* **1997**, *275*, 681−688.
(13) Dutta, P. K.; Robins, D. S. *Langmuir* **1994**, *10*, 4681−4687.
(14) Ogawa, M.; Kuroda, K. *Chem. Rev.* **1995**, *95*, 399−438.
(15) Takagi, K.; Shichi, T.; Usami, H.; Sawaki, Y. *J. Am. Chem. Soc.* **1993**, *115*, 4339−4344.
(16) Shichi, T.; Takagi, K.; Sawaki, Y. *J. Chem. Soc., Chem. Commun.* **1996**, 2027−2028.
(17) Shaw, B. R.; Deng, Y. P.; Strillacci, F. E.; Carrado, K. A.; Fessehaie, M. G. *J. Electrochem. Soc.* **1990**, *137*, 3136−3143.
(18) Shaw, B. R.; Creasy, K. E. *J. Electroanal. Chem.* **1988**, *243*, 209−217.
(19) Therias, S.; Mousty, C. *Appl. Clay Sci.* **1995**, *10*, 147−162.
(20) Mousty, C.; Therias, S.; Forano, C.; Besse, J. P. *J. Electroanal. Chem.* **1994**, *374*, 63−69.
(21) Bonnet, S.; Forano, C.; de Roy, A.; Besse, J. P. *Chem. Mater.* **1996**, *8*, 1962−1968.
(22) Kooli, F.; Chisem, I. C.; Vucelic, M.; Jones, W. *Chem. Mater.* **1996**, *8*, 1969−1977.
(23) Kanezaki, E.; Sugiyama, S.; Ishikawa, Y. *J. Mater. Chem.* **1995**, *5*, 1969−1972.
(24) Kanezaki, E.; Kinugawa, K.; Ishikawa, Y. *Chem. Phys. Lett.* **1994**, *226*, 325−330.
(25) Vucelic, M.; Moggridge, G. D.; Jones, W. *J. Phys. Chem.* **1995**, *99*, 9, 8328−8337.
(26) Moore, D. M.; Hower, J. *Clays Clay Miner.* **1986**, *34*, 379−384.
(27) Ruiz-Conde, A.; Ruiz-Amil, A.; Perez-Rodriguez, J. L.; Sanchez-Soto, P. J. *J. Mater. Chem.* **1996**, *6*, 1557−1566.

(28) Bookin, A. S.; Cherkashin, V. I.; Drits, V. A. *Clays Clay Miner.* **1993**, *41*, 558−564.
(29) Kukkadapu, R. K.; Witkowski, M. S.; Amonette, J. E. *Chem. Mater.* **1997**, *9*, 417−419.
(30) All simulations were performed using the commercially available software package Cerius^2 v.3.0 and v.3.5, Molecular Simulations Inc., 1996.
(31) Aicken, M.; Bell, I. S.; Coveney, P. V.; Jones, W. *Adv. Mater.* **1997**, *9*, 496−500.
(32) Bell, I. S.; Kooli, F.; Jones, W.; Coveney, P. V. *Materials Research Society Proceedings, Spring 1996*; 1996.
(33) Williams, S. J.; Coveney, P. V.; Jones, W. *Mol. Simul.* submitted.
(34) Allmann, R.; Jepsen, H. P. *Neues Jahrb. Mineral. Monatsh* **1969**, *12*, 544.
(35) The chosen sizes of simulation cell were found to be the optimum to give accurate results without unreasonably long processing times.
(36) Mayo, S. L.; Olafson, B. D.; Goddard, W. A., III. *J. Phys. Chem.* **1990**, *94*, 8897−8909.
(37) Stewart, J. J. P. *MOPAC version 6.0*, QCPE No. 455 **1990**, Department of Chemistry, Indiana University: Bloomington, IN, 1990.
(38) Boek, E. S.; Coveney, P. V.; Williams, S. J.; Bains, A. *Mol. Simul.* **1996**, *18*, 145−154.
(39) Rappe, A. K.; Goddard, W. A., III. *J. Phys. Chem.* **1991**, *95*, 3358.
(40) Hoover, W. H. *Phys. Rev. A* **1985**, *31*.
(41) Boek, E. S.; Coveney, P. V.; Skipper, N. T. *J. Am. Chem. Soc.* **1995**, *117*, 12608−12617.
(42) De Siqueira, A. V. C.; Skipper, N. T.; Coveney, P. V.; Boek, E. S. *Mol. Phys.* **1997**, *92*, 1−6.
(43) Kagunya, W.; Dutta, P. K.; Lei, Z. *Physcia B* **1997**, *234−236*, 910−913.